Desert-Based Absolute Calibration of Successive Geostationary Visible Sensors Using a Daily Exoatmospheric Radiance Model

Rajendra Bhatt, David R. Doelling, Daniel Morstad, Benjamin R. Scarino, and Arun Gopalan

***Abstract*—A desert daily exoatmospheric radiance model (DERM) based on a well-calibrated (reference) geostationary Earth orbit (GEO) satellite visible sensor can be used to transfer the calibration to a (target) GEO sensor located at the same equatorial longitude location. The DERM is based on the reference GEO daily radiances observed over a single pseudoinvariant calibration site (PICS) being that the daily angular conditions are repeated annually for any historical or successive colocated GEO. The GEO-specific PICSs used in the study are first inspected using the well-calibrated Aqua-MODerate Resolution Imaging Spectroradiometer (MODIS) exoatmospheric reflectances for stability. The Libyan Desert site was found to be stable within 1% over ten years. The average clear-sky daily local-noon interannual variability based on Meteosat-9 0.65-μm top-of-atmosphere radiances over the Libyan Desert is 0.74%, which implies that the combined surface and atmospheric column is invariant. A spectral band adjustment factor, based on Scanning Imaging Absorption Spectrometer for Atmospheric Cartography spectral radiances, is used to account for sensor spectral response function (SRF) differences between the reference and target GEO. The GEO reference calibration was based on the GEO/Aqua-MODIS ray-matched radiance intercalibration transfer technique. The reference Meteosat-9 DERM and ray-matched calibration consistency was within 0.4% and 1.9% for Meteosat-8 and Meteosat-7, respectively. Similarly, GOES-10 and GOES-15 were calibrated based on the GOES-11 DERM using the Sonoran Desert and were found to have a consistency within 1% and 3%, respectively.**

***Index Terms*—Geostationary visible imager calibration, pseudoinvariant calibration targets, spectral band adjustment factor (SBAF).**

I. Introduction

In THE last three decades, there has been an increased interest in the use of multiple geostationary Earth orbit (GEO) satellites for studying long-term global climate change. Products based on the International Satellite Cloud Climatology Project rely on well-calibrated GEO radiances [1]. The Clouds and the Earth's Radiant Energy System (CERES) project incorporates three-hourly GEO enhanced broad-band fluxes between CERES measurements to provide diurnally averaged fluxes [2]. These GEO operational visible imagers must be vicariously calibrated owing to an absence of any onboard calibration. An approach that uniformly calibrates all historical and current GEO sensors to the same absolute radiometric scale is important because the impact of calibration artifacts in the GEO record could be misinterpreted as change in climate.

Historical GEO sensors were vicariously calibrated using intercalibration with similar radiometric sensors or with computed exoatmospheric radiances based on the Earth's surface and atmospheric column [3]. Bright invariant desert sites were identified and characterized, particularly for temporal stability, in order to vicariously calibrate visible sensors [4], [5]. The predicted radiances as a function of angular geometry relied on a radiative transfer model based on *a priori* surface bidirectional reflectance distribution function (BRDF) and spectral signature as well as atmospheric profiles to account for atmospheric absorption at the time of measurement [6]–[8].

The predicted radiances from these invariant desert sites were improved over time and were eventually compared against recent well-calibrated polar orbiting sensors in order to establish an uncertainty in the calibration [8]. Chun *et al.* [9] used the operational MODIS surface BRDF parameter product and the Advanced Spaceborne Thermal Emission and Reflection spectral albedos to calibrate the Multifunctional Transport Satellite (MTSAT)-1R geostationary visible imager. The predicted MTSAT-1 radiances were compared against MODIS radiances and were found to have an absolute accuracy of 6%. Govaerts *et al.* [8] calibrated Meteosat-5 and Meteosat-7 to an absolute calibration accuracy of 5% by employing an approach that uses the surface BRDF and spectra as the absolute calibration reference in order to calibrate the GEO visible sensors. The greatest uncertainty in this approach is the BRDF and the spectral signature of the desert surface.

GEO sensors have been located over the same (effectively) equatorial subsatellite point over many decades, and similar daily imaging schedules provide matching solar and azimuth angular conditions on a particular day of year. If the atmosphere and surface reflectance over clear-sky desert sites were invariant and the GEO visible sensor was stable, then the daily angular observed radiances observed over one year would be effectively

Manuscript received October 12, 2012; revised April 19, 2013; accepted July 8, 2013. This work was supported by the National Aeronautics and Space Administration Earth Science Enterprise Office through the Clouds and the Earth's Radiant Energy System and the Satellite Calibration Interconsistency Programs and by the National Atmospheric and Oceanic Administration Climate Data Records Program through Grant MOA IA1-1016.

R. Bhatt, D. Morstad, B. R. Scarino, and A. Gopalan are with the Science Systems and Applications, Inc., Hampton, VA 23666 USA (e-mail: rajendra.bhatt@nasa.gov; Daniel.morstad@nasa.gov; Benjamin.r.scarino@nasa.gov; arun.gopalan-1@nasa.gov).

D. R. Doelling is with the National Aeronautics and Space Administration Langley Research Center, Climate Sciences Branch, Hampton, VA 23681 USA (e-mail: david.r.doelling@nasa.gov).

Color versions of one or more of the figures in this paper are available online at http://ieeexplore.ieee.org.

Digital Object Identifier 10.1109/TGRS.2013.2274594

identical to that of other years. It is then possible for a well-calibrated GEO visible reference sensor to intercalibrate other GEO sensors with similar spectral response functions (SRFs) that share the same subsatellite point. The BRDF is eliminated in this approach because the angular geometry used in intercalibration is based on observed radiances. The top of atmosphere (TOA) hyperspectral radiances observed over the specific pseudoinvariant calibration site (PICS) by the SCanning Imaging Absorption spectroMeter for Atmospheric CartograpHY (SCIAMACHY) can then account for SRF differences between the target and reference GEO sensors. This approach eliminates the radiative transfer computation through the atmosphere and relies on numerous observed hyperspectral radiances to account for the GEO SRF differences. Because the GEO sensors do not have onboard calibration, the GEO reference calibration is obtained by intercalibrating with MODIS, which has excellent onboard calibration based on solar diffusers, through coincident, coangled, and colocated GEO radiances [10], [11]. Calibrated SCIAMACHY hyperspectral radiances are used to normalize the SRF differences.

The concept of evaluating the temporal stability of desert targets using same-day-of-year measured TOA radiances is not new. Kizu and Kawamura used an albedo ratio between two years in order to assess the stability of the Geostationary Meteorological Satellite-3 visible sensor [12]. Grau and Torres used an iterative method to compute the annual changes in the Meteosat-7 calibration [13]. Le Borgne *et al.* [14] used daily ratios between two years using three desert sites to compute the degradation of the Meteosat-4, Meteosat-5, and Meteosat-7 visible sensors. These methods rely on the first year of daily TOA radiances as the reference calibration to evaluate the stability in successive years. If there were significant degradation during the first year, this approach would be compromised. To determine clear-sky conditions over the PICS, these methods rely on simple spatial-standard-deviation thresholds, which assume that any clouds or significant sand storm advents decrease the spatial homogeneity significantly [12], [13]. These methods do not seek pristine desert atmospheric conditions, desired by radiative transfer approaches to reduce radiance uncertainty, but rather average clear-sky conditions. Only interannual changes are not accounted for, such as stratospheric aerosols, total integrated water vapor or ozone, and changes in the dune displacements [14]. This study differs from the stability methods by using all the years of the reference GEO satellite to build the TOA radiance model, given that the GEO reference sensor record is calibrated against the Aqua-MODIS sensor. This approach has the potential to uniformly intercalibrate most historical GEO sensors.

The study is organized as follows. First, the PICS stability is verified by Aqua-MODIS exoatmospheric reflectance trends. This section also suggests other potential PICSs located over most GEO domains. In the next section, the intercalibration of the GEO visible sensor with Aqua MODIS using coincident ray-matched radiance pairs is illustrated. Thereafter, the construction of the clear-sky daily exoatmospheric radiance model (DERM) is described in detail, demonstrating that the surface and atmospheric column is invariant over time. Then, the application of the spectral band adjustment factor (SBAF), based on SCIAMACHY spectral radiances, to account for the sensor SRF differences will be addressed. Section III presents the validation of the DERM intercalibration method over the Libya-4 PICS using Meteosat-9 (reference) and Meteosat-8 (target) pairs with similar spectral responses and Meteosat-9 (reference) and Meteosat-7 (target) with rather different bandwidths. Examples including GOES-11 as reference and GOES-10 and GOES-15 as targets over the Sonoran Desert are also given in the section. Finally, a summary of the approach is provided in the conclusions.

II. Methodology

A. Selection of Invariant Sites Over the GEO Domains

Invariant sites are stable terrestrial targets wherein the reflectance remains nearly constant over time. Numerous past researchers have reported on the qualities of invariant sites [4], [5], [15], [16]. An invariant site should exhibit long-term radiometric stability, high surface reflectance, and near overhead sun to maximize the signal-to-noise ratio (SNR), high spatial homogeneity to minimize the effect of misregistration, flat spectral reflectance, and a near Lambertian surface to minimize the errors associated with BRDF effects. Also, preferable regions are aerosol free and are located at high elevations to mitigate the effects of water vapor absorption. In addition, the site should be in an arid region, thus minimizing the presence of clouds and vegetation. Given that it is unlikely that any terrestrial site can satisfy all of these criteria, the term PICSs is used to refer to those regions that remain reasonably stable over time and exhibit features resembling those described earlier [16]. Possible PICSs within each GEO domain are selected from previous studies.

The driest and most reflective PICSs are found over the Saharan and Arabian desert areas. Extensive studies have characterized multiple Saharan desert sites for use as calibration studies [4], [5], [16]–[20]. Many Meteosat calibration studies have used Saharan desert sites [7], [8], [13], [14]. The Committee on Earth Observation Satellites Infrared and Visible Optical Sensors subgroup has recommended six sites (Libya 4, Mauritania 1 and 2, Algeria 3, Libya 1, and Algeria 5) as reference standard test sites for monitoring the postlaunch radiometric performance of the spaceborne optical sensors [21]. The Libya-4 desert site has been used by the MODIS and Landsat calibration teams to monitor the stability of their visible sensors [15], [17], [22], [23]. The Libya-4 and Arabia-2 desert sites can be viewed by satellites positioned at 0° longitude and over the Indian Ocean.

For satellites positioned over the Western Hemisphere, the Sonoran Desert has been the most widely used [6], [17], [19], [22], [24]. The Sonoran Desert has been used to monitor the calibration of the Landsat [20], [22] and can be seen from both GOES-West and GOES-East positions.

Several studies have used Chinese interior desert PICSs to calibrate visible sensors [12], [19], [25]–[27], the sites of which include the Taklamakan, Badain, and Dunhuang deserts. The Badain Jaran Desert located in the central Inner Mongolia of Northern China is the most invariant site within this domain [25]. These desert sites are located much further north compared to the usual subtropical desert sites. They also have a

darker surface reflectance, which makes their SNR lower than that of the subtropical desert sites. These sites can be viewed by satellites positioned over the Indian Ocean and West Pacific.

Australian deserts have also been used as calibration targets [9], [12], [28], [29]. The Simpson Desert Aqua-MODIS nadir reflectance values show an increasing trend from 2002 to 2010 [9], [28] and then a sharp decline in reflectance thereafter [28]. Schmidt *et al.* reported that the five-year trend in the Tinga Tingana time series, the most stable of the Australian PICSs, is strongly affected by an episode of local vegetation growth in 1996–1997 [29]. Seemingly, there are rather few Australian deserts entirely void of vegetation and that are not plagued by interannual rainfall events. The Australian desert region would be suitable for satellites positioned over the Western Pacific.

Calibrations based on deserts are only as good as the stability of the target, which must be verified. The temporal stability of these regions is demonstrated individually using ten years of clear-sky MODIS data acquired at these sites. The Aqua-MODIS Collection-6 Level-1b Band-1 (0.65 μm) data are used for this purpose. Aqua MODIS is used because it is stable to within 1% per decade and is better characterized and more stable compared to Terra MODIS [23]. TOA observed near-nadir (viewing zenith angle $< 10°$) Aqua reflectance data over these sites are normalized by a site-specific BRDF model that is based on the first three years of the Aqua record, which is the most stable period. The BRDF approach is semiempirical and is based on a linear combination of two kernel functions as described by Roujean *et al.* [30]. Only nadir TOA reflectances are used to derive the BRDF, which models the TOA reflectance as a function of solar zenith angle (SZA), as used in the approach of Angal *et al.* [17]. Only reflectances from clear-sky conditions are used. Such a condition is determined by a spatial uniformity test, which follows the same test as the DERM and is described in more detail in the next section. Fig. 1 shows the individual Aqua-MODIS near-nadir normalized PICS reflectances, which have a near-nadir sampling frequency of 16 days. The ten years (July 2002 to December 2012) of normalized reflectances are then used to assess the stability of the site.

The PICSs described in this section are listed in Table I by their center latitude and longitude, along with the extent of the region of interest (ROI). The ten-year mean Aqua-MODIS reflectance, spatial homogeneity based on the 1-km pixel-level reflectance spatial standard deviation in the ROI, and temporal stability based on the standard deviation of all of the 16-day observed reflectances are also given in Table I. The Libya-4 and Sonoran desert sites are stable within 1% based on Aqua-MODIS observations and can be used to demonstrate the DERM. Table II provides the equatorial longitude locations of the successive operational satellites and the view angle to the PICS listed in Table I. Given that the GEO satellites have been positioned over the same approximate location successively, and usually with the same imaging frequency, it is possible to construct a DERM for each PICS.

B. GEO Reference Calibration Based on Aqua-MODIS Intercalibration

The absolute calibration of the reference GEO is obtained from the intercalibration of the GEO and Aqua-MODIS

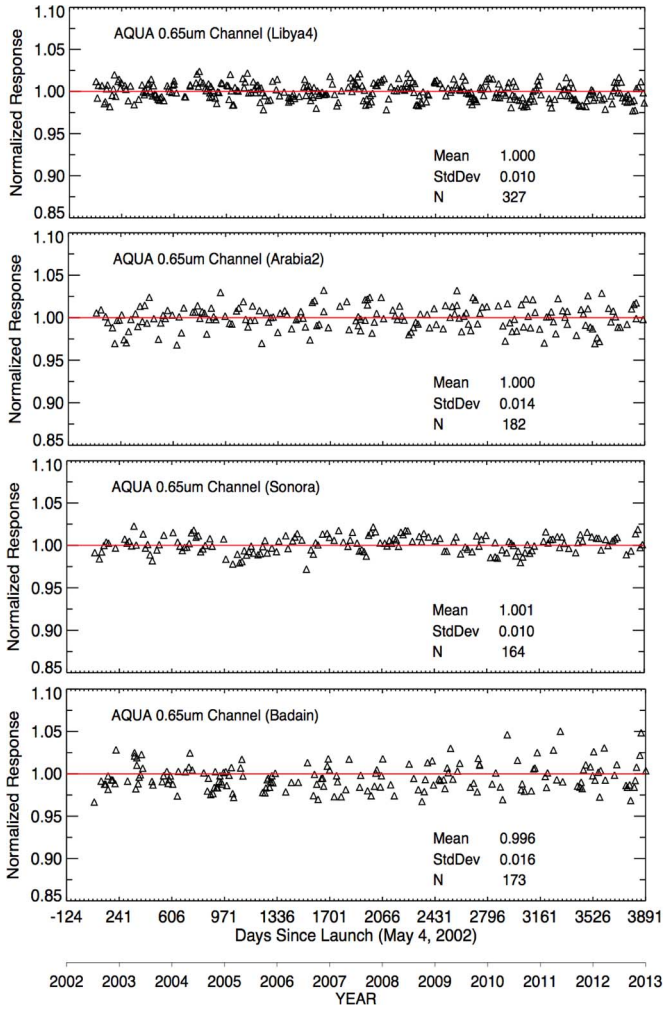

Fig. 1. Normalized TOA near-nadir Aqua-MODIS 0.65-μm observed clear-sky reflectances over (from top to bottom panels) Libya-4, Sonora, Arabia-2, and Badain PICSs from 2002 to 2012. The mean, standard deviation, and number of observations over the record are given for each PICS.

0.65-μm band, which has excellent onboard calibration as mentioned in the previous section. The Aqua-MODIS calibration is transferred using coincident (within 15 min) angular matched radiance pairs over an equatorial ocean domain centered on the GEO subsatellite point. The matched radiance pairs are linearly regressed on a monthly basis. The procedure is described in detail by Minnis *et al.* [10]. The reference GEO gain is then the factor needed to multiply the GEO count, which is proportional to radiance, after adjusting for the space count. The SRF difference between the GEO and MODIS channels is accounted for by using SCIAMACHY hyperspectral radiances as outlined by Doelling *et al.* [31]. Essentially, all SCIAMACHY footprints located over the equatorial ocean GEO domain are used to compute pseudo GEO and MODIS radiances by integrating the GEO and MODIS SRFs with the SCIAMACHY hyperspectral radiances. For this study, we processed the SCIAMACHY Level-1B data (SCI_NL_1P, Version 7.03) produced with the European Space Agency-distributed data calibrator in order to extract the SCIAMACHY measurements from 240 to 1750 nm. All of the pseudo GEO and MODIS radiance pairs are regressed to derive the SBAF. The SBAF is then used to adjust the Aqua-MODIS radiance to derive an equivalent GEO radiance.

TABLE I
PICSs Inspected in This Study Along With Their Location and Areal Extent, the Ten-Year Mean (July 2002 to December 2012) Aqua-MODIS Band-1 (0.65 μm) Near-Nadir Clear-Sky Reflectance, the Spatial Homogeneity Based on the 1-km Pixel-Level Reflectance Spatial Standard Deviation in the ROI, and the Temporal Stability Based on the Standard Deviation of All of the 16-Day Observed Reflectances

No.	PICS	Center (Lat/Lon)	ROI	Aqua-MODIS 0.65 μm		
				Mean reflectance	Homogeneity (%)	Stability (%)
1	Libya-4	28.6°/23.4°E	0.5°x0.5°	0.46	1.4	1.0
2	Sonora	32.0°/114.5°W	0.2°x0.2°	0.32	2.5	1.0
3	Arabia-2	20.1°/51.0°E	0.5°x0.5°	0.41	1.3	1.4
4	Badain	40.1°/101.8°E	0.4°x0.4°	0.22	3.2	1.6
5	Taklimakan	39.8°/80.2°E	0.4°x0.4°	0.27	6.5	3.3
6	Simpson	-24.1°/137.4E°	0.7°x0.9°	0.22	8.6	9.4

TABLE II
GEO Satellites Listed as a Function of Equatorial Longitude Position. The GEO View Angle From the Longitude Position to the PICS Is Listed in Table I

GEO Satellites	GEO Longitude	PICS view angle (deg) to GEO satellite					
		1	2	3	4	5	6
Meteosat 1-9	0° E	42.1		61.7			
Indian Meteosat 5,7	~60° E	49.5		24.6	65.3	53.0	
(West) FY2 D	86° E				50.0	47.2	62.3
(East) FY2 C,E	105° E				46.9	52.7	46.0
GMS 1-5, MTSAT 1-2	140° E				60.8	75.9	30.0
(West) GOES 3,4,6,9,10,11,15	135°W		43.5				
(East) GOES 2,5,7,8,12,13, 14	75°W		56.4				

C. Derivation of the DERM

If the PICS seasonal variation is consistent over time, the invariance suggests the possibility of constructing a clear-sky DERM. The DERM should be based on multiple years of consistently calibrated geostationary data and should be suitable for predicting the TOA radiance for the site. Fig. 2 shows over five years (April 2007 to March 2011) of clear-sky daily TOA observations of Libya 4 from the Meteosat-9 0.65-μm channel. Meteosat-9 is operated by the European Organisation for the Exploitation of Meteorological Satellites and was a prime geostationary satellite at 0° longitude from April 2007 to January 2013. It scanned the Libya-4 PICS with a viewing zenith angle of 42.1°. The 10:30 GMT image time, which is close to local noon, is used in this study. Local noontime is chosen to ensure the maximum SNR. The Meteosat-9 visible pixel (3-km nominal) raw counts acquired over the ROI are averaged after subtracting the known space count value of 51 [32]. The mean raw count is then converted to absolute TOA radiance using the calibration gains derived for Meteosat-9 through ray-matching intercalibration with Aqua MODIS [10], [11]. The consistent repeating cycle of the TOA radiance every year suggests that the ground site and the atmosphere above it form an invariant system together, which can be characterized using only the clear-sky TOA observations from a satellite.

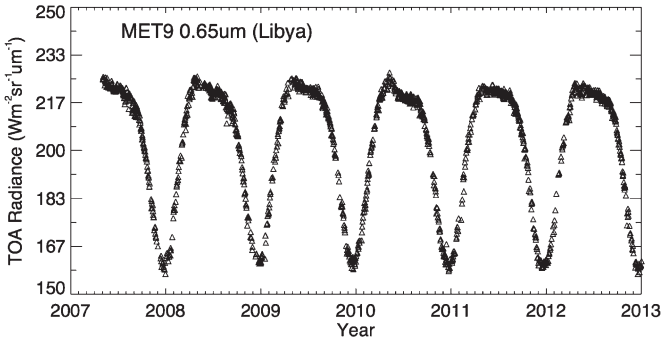

Fig. 2. Meteosat-9 10:30 GMT image clear-sky daily TOA radiances derived over Libya 4.

Clear-sky scenes are identified daily using a spatial-standard-deviation threshold of the target site, which captures the mean atmospheric turbidity conditions. Cloudy and significant aerosol events should be filtered using this threshold. On a clear-sky day, the desert pixels are homogeneous, resulting in a low spatial standard deviation [7], [12], [13]. The spatial standard deviation of Meteosat-9 visible pixels over Libya 4 is displayed in Fig. 3. A spatial-standard-deviation clear-sky count threshold of 5 counts was selected visually. The mean spatial standard deviation of clear-sky days is 3.5 counts, which

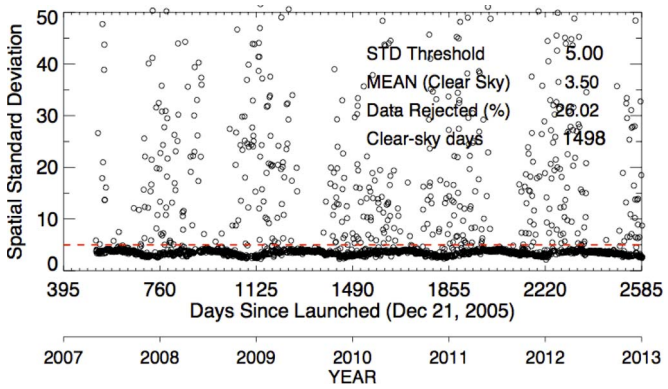

Fig. 3. Spatial standard deviation, in digital counts, of the Meteosat-9 visible pixels over Libya 4. Of the daily points, 2% exceeded a spatial standard deviation of 50 counts.

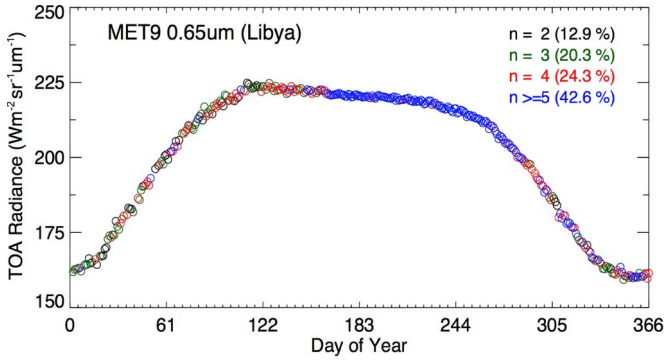

Fig. 4. Meteosat-9 clear-sky DERM of Libya 4. Here, n stands for the number of daily observations averaged for each day-of-year TOA radiance.

is less than 1% of the averaged spatial raw count, indicating that Libya 4 is spatially homogeneous. Notice that most years have consistent spatial standard deviations. The cloudy years have spatial standard deviations much greater than the minima, indicating the robustness of the clear-sky spatial method for selecting clear-sky days. Owing to the presence of clouds, 26.02% of Meteosat-9 data are found unusable for creating a DERM of Libya 4.

The next steps are to average the same-day-of-year TOA radiances and derive the DERM (see Fig. 4). Each point in Fig. 4 is the average of the measured Meteosat-9 TOA radiances for that particular day from 2007 to 2012 and is color-coded with the number of points averaged. More than 80% of the days have three or more years available for each day to derive the DERM. Fig. 5 shows the interannual variability calculated using the standard deviation of the multiple years of observations made for each existing day in the DERM. The majority of the existing days in the DERM have an interannual variability of less than 1%. During winter months, when the SZA is high, the decreased SNR leads to more days of variability over 1%. On average, the variability of a particular day observation in the DERM is about 0.74%.

D. Spectral Band Corrections

The DERM can be applied directly if the SRFs of the reference and target sensors are similar. However, this similarity is rare, and an SBAF must be applied when the sensor SRFs

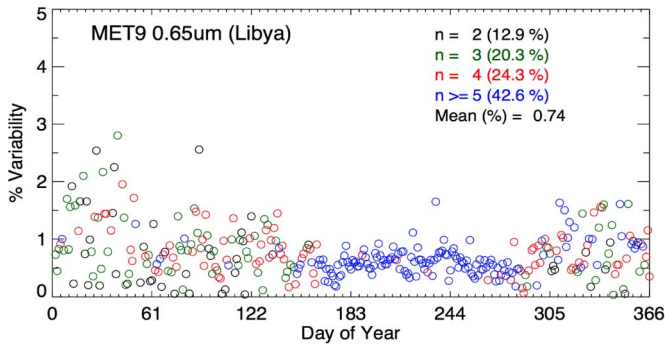

Fig. 5. Daily interannual variability in the observed Meteosat-9 DERM radiance over Libya 4 from five years of clear-sky daily TOA radiances.

differ. This difference in observation is scene dependent and can be quantified empirically by the knowledge of the spectral profile of the target [20]. For this study, the high-resolution reflected solar spectra measured by SCIAMACHY over the PICS are used to derive the SBAF needed to account for the spectral band differences between the GEO instruments. This method follows the technique described by Doelling *et al.* [31]. SCIAMACHY is on the Environmental Satellite, which has a local equator crossing time of 10:00 A.M. This study uses 1-s integration of the SCIAMACHY Level-1B (SCI_NL_1P, Version 7.03) data that have a spatial resolution of 30 km along track by 240 km across track for the nadirlike scans. Because the SCIAMACHY footprint is much larger than the Libya-4 ROI, a sensitivity study was performed to determine the effect of the spatial mismatch on the SBAF. First, using the same clear-sky days that identified the near-noon (10:30 GMT) Meteosat-7 Libya-4 daily TOA radiances between 2003 and 2010, we computed the SBAF by selecting all the clear-sky SCIAMACHY footprints for which the 30-km-by-240-km footprint center was contained within the Libya-4 ROI, as defined in Table I. There was a total of 119 SCIAMACHY footprints between 2003 and 2010 that satisfied this criterion. Next, we defined an extended 1.5° by 1.5° ROI over the Libyan site with its center at 28.75° latitude and 23.25° longitude and then collected all the clear-sky SCIAMACHY footprints for which the centers were within the new ROI. As a result, an increased sample of 899 SCIAMACHY footprints was used to compute the SBAF over Libya 4. Fig. 6 shows the Libya-4 ROI (red), the extended ROI (green), and six consecutive SCIAMACHY footprints (blue) from one orbit over the Libya-4 PICS. The SCIAMACHY-footprint centers are marked with an "x." The sixth SCIAMACHY footprint is marked with a dotted line because its center does not fall within any of the two ROIs, and therefore, it is not used in computing an SBAF. Fig. 7 shows the average and standard deviation of the SCIAMACHY reflectance spectra for the Libya-4 ROI and the extended ROI. A comparison of the two spectra shows that they have a mean absolute difference of only 0.6%, which suggests that the entire Libyan Desert has a very uniform spectral signature. For both cases, the TOA Libyan Desert reflectance spectrum variability is within ∼0.02 for wavelengths less than 0.7 μm and ∼0.05 for wavelengths that are greater than 0.7 μm. This low variability demonstrates that, even in the near IR, in which water vapor absorption is strong, the TOA

Fig. 6. Libya-4 ROI (red), the extended ROI (green), and six consecutive SCIAMACHY footprints (blue) with their centers marked with "x." SCIAMACHY footprint 4 is used to compute the SBAF over Libya 4, whereas the footprints 1 through 5 are used to compute the SBAF over the extended ROI.

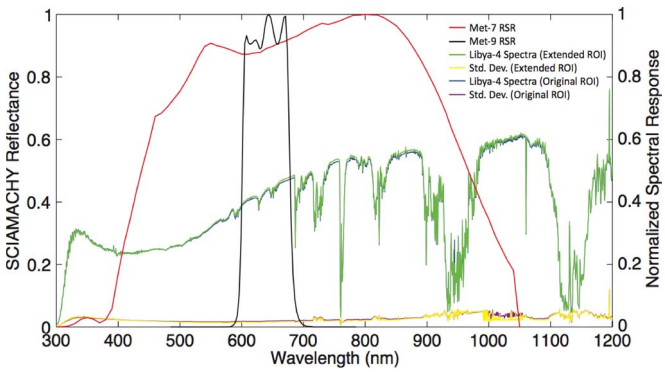

Fig. 7. Normalized SRFs, or relative response functions, of (red line) Meteosat-7 and (black line) Meteosat-9, along with the (blue line) 2003–2010 mean and (purple line) standard deviation of the 119 SCIAMACHY-footprint clear-sky TOA reflectance spectra over Libya 4. The mean and standard deviation of the 899 SCIAMACHY clear-sky TOA reflectance spectra over the extended ROI are shown with the green and yellow lines, respectively. The two mean spectra are close with a mean difference of only 0.6%. The Meteosat-8 SRF is not specifically shown, as it is nearly identical to that of Meteosat-9.

spectrum is stable over seven years and for all seasons. The comparison of the SBAF derived from the two sets of SCIAMACHY footprints is discussed in the next paragraph.

Meteosat-8 and Meteosat-9 have almost identical SRFs for the 0.65-μm channel, signifying practically no need for an SBAF correction between the two. Fig. 7 indicates that the Meteosat-7 bandwidth is much larger than those from Meteosat-8 and Meteosat-9 and is centered more toward 0.75 μm. Therefore, an SBAF must be computed for the Meteosat-7 and Meteosat-9 pair in order to transfer the calibration of the reference (Meteosat-9) to the target (Meteosat-7). The SBAF is determined by first convolving the SCIAMACHY spectra of Libya 4 with the SRFs of Meteosat-7 and Meteosat-9, thereby estimating the pseudoimager radiances for both sensors. The Meteosat-7 pseudoradiances are then regressed against the Meteosat-9 pseudoradiances, and the forced slope (regression through zero) is used as the SBAF for this pair. Fig. 8 (left) shows that the SBAF for the Meteosat-9 and Meteosat-7 pair is 0.7745, which is yielded from a combination of the spectral signature of the incoming solar radiation (decreasing with wavelength after 0.6 μm), the increasing surface reflectance with wavelength, the strong water vapor absorption bands in the near IR, and the sensor SRF band. The estimated standard error of the forced regression slope is 1.43%, which is also a quantitative measurement of the uncertainty in the SBAF. This process is repeated again to compute the Meteosat-9-to-Meteosat-7 SBAF using the larger set of the SCIAMACHY samples (899 footprints) over the extended ROI. Fig. 8 (right) shows that the new SBAF is 0.7769, whereas the uncertainty remains practically the same as before. The two SBAFs have a difference of only 0.3%, which indicates that the spatial mismatch of SCIAMACHY footprints over Libya 4 has minimal impact on the computation of the SBAF. The SBAF regression plot for the 899 samples also indicates an apparent seasonal cycle in the SBAF. Therefore, the SBAF regressions were performed seasonally using all of the 899 SCIAMACHY samples, thereby reducing the standard error of the regression to less than 1% for all seasons except winter, for which the standard error was 1.22%. Owing to the dependence of SBAF on season, the desert DERM relies on the seasonal SBAF.

E. GEO DERM Transfer of Calibration

Once the PICS DERM is created, it is ready for use in calibrating other GEO sensors that preceded or succeeded the reference GEO sensor in the same geostationary orbit. The relationship between the TOA radiance, the measured raw count, and the calibration gain of a GEO sensor, for the examples given in the next section, is given by the following equation:

$$\text{DERM SBAF radiance} = \text{Gain} \times (\text{Raw count} - \text{Space count}). \quad (1)$$

The daily gain is the necessary factor needed to multiply the GEO count after subtracting the offset to obtain the reference DERM after applying SBAF. The DERM radiance is normalized by the cosine of the SZA to take into account the small time difference between the reference and the target GEO. The daily calibration gains are averaged on a monthly basis, and a trend is found to track the radiometric performance of the sensor over time.

F. GEO DERM Calibration Uncertainty

The GEO DERM intercalibration uncertainty is the sum of the GEO reference calibration and the DERM calibration transfer uncertainty. The GEO reference calibration was based on monthly Aqua-MODIS and GEO ray-matched radiance pair regressions. The Aqua-MODIS/GEO ray-matching calibration uncertainty is the combination of the Aqua-MODIS absolute calibration accuracy, the ray-matching error, and the Aqua-MODIS and GEO SBAF uncertainty. The Aqua-MODIS absolute calibration uncertainty is within 1.64% [33] and is based on the ground-to-orbit calibration transfer uncertainty analysis. If the ray-matching intercalibration method were perfect, then the monthly variability would mirror only the instrument

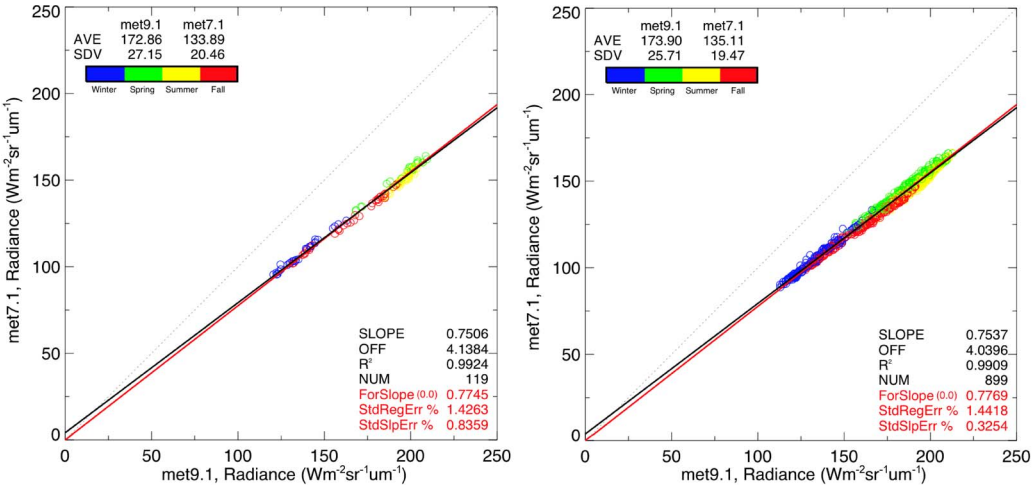

Fig. 8. Regressions of SCIAMACHY pseudo clear-sky footprint Meteosat-7 0.65-μm and Meteosat-9 0.65-μm radiances over (left) Libya 4 and the (right) extended ROI. The radiances are color coded according to season.

calibration drift. The monthly variability of the ray-matched gains is then the uncertainty, which is defined by the standard error about the trend regression. The Aqua-MODIS-to-GEO SBAF uncertainty for ray matching is computed the same way as over the deserts from the regression of all the SCIAMACHY-footprint pseudoradiance pairs over the equatorial GEO domain during 2003–2010. One SCIAMACHY 30-km-by-240-km footprint is nearly spatially representative of a 50-km region used to derive the radiance pairs in the ray-matching intercalibration. The standard error of the regression ideally provides a representative interannual and seasonal variability, about the SBAF, of the GEO spectra radiance measured, not observed, by MODIS.

Four major sources of uncertainty are identified for the DERM calibration transfer methodology itself. First, there is uncertainty associated with the reference PICS DERM, which is used to predict a daily TOA radiance for a target GEO. This is contributed jointly by the PICS temporal stability as well as the annual atmospheric condition change over the site. The mean interannual variability of the DERM radiance (discussed before) is the estimate of this uncertainty. The second contribution to the uncertainty is from the computation of the SBAF for the reference and target GEO pair. This uncertainty component is estimated from the standard error of the SBAF regression slope of all the 2003–2010 SCIAMACHY-footprint pseudoradiance pairs over the PICS, which should capture the out-of-band DERM spectral variability. Although the ROI and SCIAMACHY geometry may not be aligned, every effort has been made to identify SCIAMACHY footprints that represent the ROI. The navigation accuracy is identified as the third source of uncertainty in the DERM method. This can be estimated by assuming a typical navigation error and shifting the navigation by that amount in eight directions from the ROI. The standard deviation of the eight mean reflectances is the uncertainty factor. Usually, small ROIs have the greater navigation uncertainty because a navigation shift results in a greater fraction of GEO pixels that do not observe the ROI. Fourth, the monthly variability of the GEO DERM gain about the calibration trend line also contributes to the DERM uncertainty. This contribution is directly related to the regression of the monthly DERM gain time series data and is estimated from the standard error of the regression. A small standard error indicates high confidence in the DERM predicted gain for a given time. Longer time records usually also result in smaller standard errors. Finally, the total DERM calibration uncertainty is obtained by combining the individual contributions in quadrature.

G. GEO DERM Calibration Validation

The validation of the GEO DERM is a self-consistency test. The GEO DERM target calibration is compared to the GEO-target/Aqua-MODIS ray-matched intercalibration. Aqua MODIS is used to intercalibrate both the reference GEO for DERM and the target GEO for comparison. If the Aqua-MODIS ray-match intercalibration were perfect, then any GEO target DERM and ray-match calibration gain difference is due to the DERM methodology. If the gain difference is well within the combined DERM and GEO target ray-matched uncertainty, the self-consistency test validates the DERM methodology. For this self-consistency check, the Aqua-MODIS absolute calibration is not needed in the uncertainty analysis. However, the absolute calibration of the DERM method needs to include the Aqua-MODIS uncertainty.

III. Results and Discussions

The successive GEO desert DERM intercalibration technique is evaluated in three examples. The first example transfers the Meteosat-9 Libya-4 DERM to Meteosat-8, for which SRFs are nearly identical. The second example transfers the same Meteosat-9 DERM to Meteosat-7, for which the SRFs are very different, thereby determining the effectiveness of the SBAF. The third example transfers the GOES-11 Sonoran DERM to GOES-10 (similar SRFs) and GOES-15 (different SRFs) illustrating the technique over another GEO domain and sensor.

A. Meteosat-8 Calibrated With Meteosat-9 DERM

The Meteosat-9 DERM was applied to the Meteosat-8 mean raw count over the Libyan Desert region from the 10:30 GMT

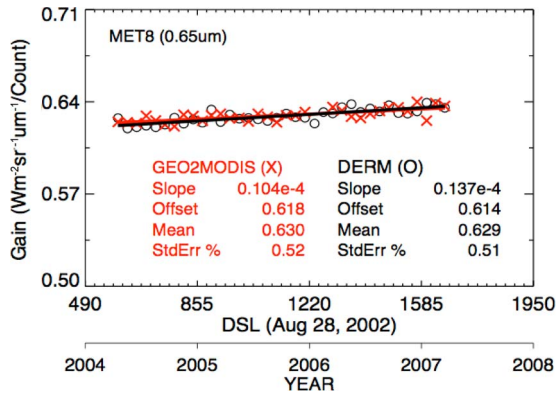

Fig. 9. Comparison of Meteosat-8 visible channel (0.65 μm) monthly radiometric gains derived from Aqua-MODIS/Meteosat-8 ray matching (red Xs: MODIS-to-GEO) and the Meteosat-9 reference Libya-4 desert DERM (black circles: desert). Linear regression statistics of the monthly gains are also given.

image time to derive a daily gain using (1). The observations are not perfectly coangled because Meteosat-8 was operated at 3.4° longitude west of Meteosat-9. This disparity results into a viewing angular difference of 0.97° over Libya 4. In order to account for this viewing angle difference, a TOA BRDF model [30] of Libya 4 was developed based on ten years of Aqua-MODIS band 1 reflectance data with the viewing zenith angle between 0° and 50°. The Meteosat-9-to-Meteosat-8 TOA radiance correction factor for Libya 4 as estimated from the Aqua-MODIS BRDF model described in Section II is 0.9995 (0.05% correction), which is insignificant. The Meteosat-8 daily gains obtained from (1) are then averaged on a monthly basis, and a trend is established. The monthly gains are compared with the ray-matched calibration for Meteosat-8/Aqua MODIS during the same time period. Fig. 9 displays the DERM and ray-matched monthly gains for Meteosat-8 and the associated linear regression coefficients, the lifetime mean gains, and the standard error about regression. All of the uncertainties stated in Section II-F are listed in Table III. In this case, Meteosat-8 and Meteosat-9 have nearly the same SRF, resulting in an SBAF uncertainty of zero. The Aqua-MODIS-to-Meteosat-9 ray-matching calibration uncertainty is 0.98%. The DERM uncertainty is only 0.74%, which implies that the Libya-4 desert and atmospheric column is an excellent transfer medium. The Libya-4 navigation uncertainty is 0.1% using a 3-km navigation shift, whereas the uncertainty in the Meteosat-8 DERM calibration trend is 0.51%. The total absolute calibration uncertainty of Meteosat-8 using the DERM approach is 2.11%, which is computed from the quadrature sum of all individual contributions listed under the Meteosat-9/8 column of Table III. The DERM and ray-match gain difference is 0.16%, which is well within the uncertainty of either methods, and is presented in Table IV. These results show the effectiveness of transferring calibration via the DERM, validating that the PICS is stable and the DERM approach is robust.

B. Meteosat-7 Calibrated With Meteosat-9 DERM

To determine the effectiveness of the desert SBAF in the Meteosat-9 DERM approach, the SBAF was applied to the Meteosat-7 (at the 0° longitude location) visible counts over the Libyan Desert region from the 10:30 GMT image time, thus deriving daily gains (1). There is a 10-min time difference between the Meteosat-9 and Meteosat-7 Libya-4 scan times; however, the maximum SZA difference between the Meteosat-9 and Meteosat-7 is only 1.5°. To account for this difference, the DERM radiance was normalized by the cosine of the SZA. The clear-sky spatial threshold of 1.5 counts (8-b count resolution and 4.5-km nominal spatial resolution) was used to identify Meteosat-7 clear-sky days. The average clear-sky spatial standard deviation was 0.70, and nearly 80% of all days considered were identified to be clear. The space count for Meteosat-7 was derived independently by the authors by averaging the pixel-level visible counts over the dark portion of the Earth demarcated with an SZA $> 110°$ in the 17:30 GMT image. The analysis showed that the Meteosat-7 space count has a fairly stable value of 4.9 throughout the lifetime. The Meteosat-7/Meteosat-9 Libya-4 seasonal SBAF, described in Section II-C, was applied to the daily radiances from the DERM in (1).

Fig. 10 compares the Meteosat-7 monthly gains derived from Aqua-MODIS ray matching and the DERM. The DERM monthly gains of Meteosat-7 exhibit some residual seasonal behavior, presumably caused by the interannual aerosol and water vapor difference in the Meteosat-7 broad-band channel not captured by the seasonal SBAF corrections. The Meteosat-7 DERM calibration trend uncertainty is 0.92% compared with the Meteosat-8 DERM of 0.51%, suggesting that the atmospheric column for the Meteosat-7 spectral band is causing most of the variability in the monthly gain. During the 2002–2006 overlapping Aqua time frame, the Meteosat-7 mean DERM gain is 2.222, and the gains derived from the two approaches agree within 1.86% (see Table IV). The uncertainty analysis is performed following Sections II-F and III-A, and the observed difference between the ray-matching and DERM gains is within the uncertainty limit of either approaches (see Table IV). This self-consistency check validates the SCIAMACHY-based SBAF approach of both methods and that the DERM is capable of intercalibrating over a wide range of SRFs in the visible spectrum that is common among operational GEO sensors.

C. GOES-10 and GOES-15 Calibrated With GOES-11 DERM

The GOES satellites are operated by the National Oceanic and Atmospheric Administration over two prime locations: GOES-East (75° W longitude) and GOES-West (135° W longitude). The DERM approach was applied to calibrate the GOES-10 and GOES-15 visible sensors using the reference GOES-11 DERM derived from five years of calibrated GOES-11 TOA radiances over the Sonoran Desert. The GOES-11 data were acquired from the 19:30 GMT Northern Hemisphere image, near local noon at the Sonoran desert location. GOES-11 was operational at 135° W longitude between June 2006 and December 2011, and GOES-10 was operational at the same longitude from July 1998 through June 2006. In December 2011, GOES-15 replaced GOES-11 and became the prime operational GOES-West satellite. These three sensors

TABLE III
LIST OF VARIOUS UNCERTAINTIES INVOLVED IN THE GEO DERM REFERENCE-TO-TARGET CALIBRATION TRANSFER. ALL UNCERTAINTIES ARE ESTIMATED AT 1-SIGMA LEVEL

Reference/Target GEO	MET-9/8	MET-9/7	GOES-11/10	GOES-11/15
Aqua-MODIS absolute calibration uncertainty	1.64%	1.64%	1.64%	1.64%
Aqua-MODIS to reference GEO ray-matching calibration uncertainty (transfer + SBAF)	0.98%	0.98%	1.8%	1.8%
Reference DERM radiance uncertainty	0.74%	0.74%	1.20%	1.20%
PICS SBAF uncertainty	0	0.33%	0.18%	1.22%
Navigation uncertainty (1-pixel shift in all directions)	0.1%	0.1%	0.4%	0.4%
DERM calibration trend uncertainty	0.51%	0.91%	0.83%	0.57%
Total calibration uncertainty	**2.11%**	**2.67%**	**2.87%**	**3.06%**

TABLE IV
GEO DERM REFERENCE-TO-TARGET CALIBRATION TRANSFER AND THE MODIS REFERENCE-TO-GEO CALIBRATION TRANSFER GAINS AND UNCERTAINTIES

GEO Satellite	DERM		Ray-Matching		Gain difference (%)
	Gain	Uncertainty (%)	Gain	Uncertainty (%)	
Meteosat-8	0.629	2.11	0.630	1.74	0.16
Meteosat-7 (2003-2007)	2.222	2.67	2.264	2.92	1.86
GOES-10 (2000-2003)	0.834	2.87	0.842	2.41	0.95
GOES-15 (2011-2013)	0.727	3.06	0.747	2.07	2.68

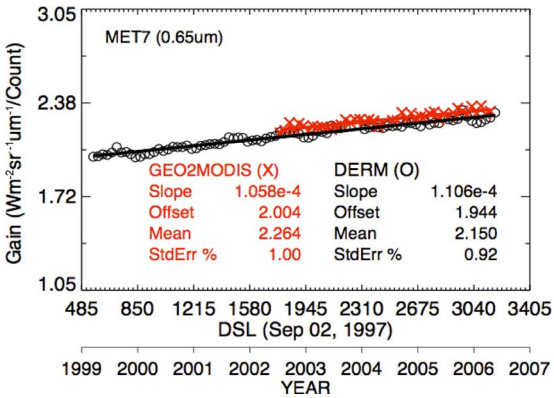

Fig. 10. Comparison of Meteosat-7 visible channel (0.75 μm) monthly radiometric gains derived from Aqua-MODIS/Meteosat-7 ray matching (red Xs: MODIS-to-GEO) and the Meteosat-9 reference Libya-4 desert DERM (black circles: desert). Linear regression statistics of the monthly gains are also given.

thus make a good illustrative case to highlight the usefulness of the DERM approach in transferring the reference GEO calibration to both historical and future collocated GEOs. During their operational lifetimes at the GOES-West position, both GOES-10 and GOES-11 viewed the Sonoran Desert at a viewing zenith angle of 43.5° and had the same operational imaging schedule, providing exact SZA and azimuth angle daily matches. The same angular conditions and imaging schedule are now repeated by GOES-15 at the GOES-West position. A constant space count of 29 is used for all three GOES imagers [34]. Based on the visual inspection of the spatial-standard-deviation profile of the Sonoran Desert ROI, as observed by GOES-11, a threshold of 8 (10-b count resolution and 1.0-km-by-0.6-km nominal spatial resolution) was used to filter cloudy scenes from the GOES-11 data set. The mean standard deviation on a clear-sky day was 5.1 counts. The statistics showed that the average interannual variability of a daily TOA radiance in the DERM of the Sonoran Desert is 1.20%, and 85% of all DERM days were derived from three or more years of radiances. The Sonoran Desert is also 30% darker than Libya 4 and has a smaller ROI with greater spatial variability (see Table I), suggesting a smaller SNR. The stability of the Sonoran Desert is rather similar to that of the Libya-4 site. This example thus also allows for a comparison of desert quality on the DERM.

Unlike Meteosat sensors, all GOES imagers have mostly similar SRFs extending from 0.5 to 0.8 μm, except for the most recent GOES sensors (GOES-13, GOES-14, and GOES-15) which only encompass wavelengths up to 0.7 μm. A feasibility study on using the large SCIAMACHY footprints over the Sonoran Desert, in order to compute the SBAF for the

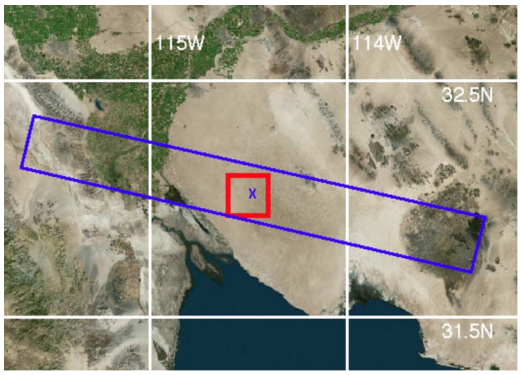

Fig. 11. (Red) Sonora Desert ROI along with the (blue) SCIAMACHY footprint.

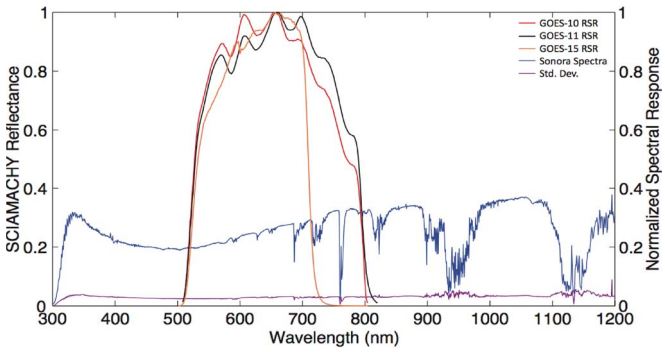

Fig. 12. Normalized relative spectral response (RSR) of (red line) GOES-10, (black line) GOES-11, and (orange line) GOES-15, along with the 2003–2010 (blue line) mean and (purple line) standard deviation of the 24 SCIAMACHY-footprint clear-sky TOA reflectance spectra over the Sonoran Desert.

DERM-based calibration of GOES sensors, was performed. All clear-sky (based on the same days as the GOES-11 reference) SCIAMACHY footprints having centers inside the Sonoran Desert ROI are identified during the 2003–2010 time frame. Owing to the location and size of the ROI, only a certain orientation of the SCIAMACHY 30-km-by-240-km footprint satisfies the criterion, thus leading to a very small sample of 24 footprints. Fig. 11 shows the Sonora Desert ROI (red) and one valid SCIAMACHY footprint that includes the Sonora ROI and extends further in the east and west directions, covering some vegetation and rocky surfaces. The SCIAMACHY footprint therefore may not yield the true reflectance spectra of the Sonoran Desert, but it is not likely to be significantly different (see next paragraph) from it, given that the major contribution to the SCIAMACHY footprint is coming from the bright desert surface. Therefore, the SCIAMACHY-based SBAF is still useful in minimizing the spectral band difference effects in the DERM intercalibration of GOES sensors. The effectiveness of the SBAF based on the 24 SCIAMACHY footprints over the Sonoran Desert is discussed next.

The mean of the 24 SCIAMACHY-clear-sky-footprint spectral-reflectance values over the Sonoran Desert is shown in Fig. 12 along with the SRFs of GOES-10, GOES-11, and GOES-15 visible bands. The associated spectral-reflectance standard deviation is on the order of 0.03 ($\sim$10%) over most of the visible spectra, which is higher than that of Libya 4, and is expected because of the limited SCIAMACHY samples and

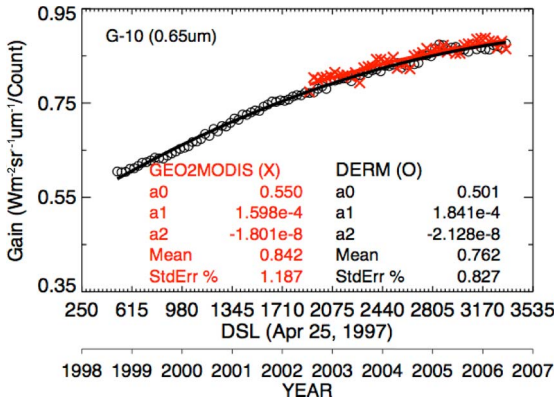

Fig. 13. Comparison of GOES-10 visible channel (0.65 μm) monthly radiometric gains derived from Aqua-MODIS/GOES-10 ray matching (red Xs: MODIS-to-GEO) and the GOES-11 reference Sonoran Desert DERM (black circles: desert). Linear regression statistics of the monthly gains are also given.

partial presence of variable scene types, including vegetation. However, the spectra do not seem to be significantly impacted by vegetation, otherwise one would expect a noticeable increase in the reflectance near IR beyond 0.7 μm. The reflectance spectra computed over the Sonoran Desert closely resemble, in shape, the desert spectra computed over Libya 4 (see Fig. 7), but are darker in magnitude as expected. Owing to the lack of sampling, no seasonal SBAF was derived for the GOES sensor pairs. Given the similarity between the GOES-10 and GOES-11 SRFs, the SBAF is 1.004, and the SBAF uncertainty is 0.18% based on 24 footprints. GOES-11 and GOES-15 are found to have the largest spectral band dissimilarity among the GOES sensors operated at the GOES-West position during the MODIS time frame. The computed SBAF for this pair is 1.029 with an uncertainty of 1.2%. This is the highest SBAF uncertainty discussed in this paper. Because the GOES SRFs do not contain any strong water vapor absorption lines, most of this uncertainty is believed to lack a seasonal SBAF due to inadequate SCIAMACHY sampling, which may not be sufficient to account for the range of natural seasonal variability in the SBAF.

Fig. 13 shows the GOES-10 DERM and Aqua-MODIS ray-matched monthly mean gains and associated second-order regression. The navigation error uncertainty, which was derived using a 2-km navigation shift, is 0.4%, which is expected given the doubled spatial variability compared to Libya 4 (see Table I), and the ROI encompasses 16% of the area. All other sources of uncertainty are listed in Table III. For the overlapping time frame between 2003 and 2006, the means of the two sets of gains agree within 1% (see Table IV), which is well within the uncertainty of either the DERM or ray-matching methods (see Sections II-F and III-A), signifying a good consistency between the two methods.

The results from the DERM and Aqua-MODIS ray-matched calibration of GOES-15 are plotted in Fig. 14. The DERM monthly gains are plotted with and without the application of the SBAF for comparison. It is evident from the figure that, without the spectral corrections, there is a systematic bias of 5.4% between the ray-matching and DERM calibration trends. The application of the SCIAMACHY-based SBAF successfully reduces the bias to half, which is a significant improvement. The remaining bias ($\sim$2.7%), however, is within the uncertainty

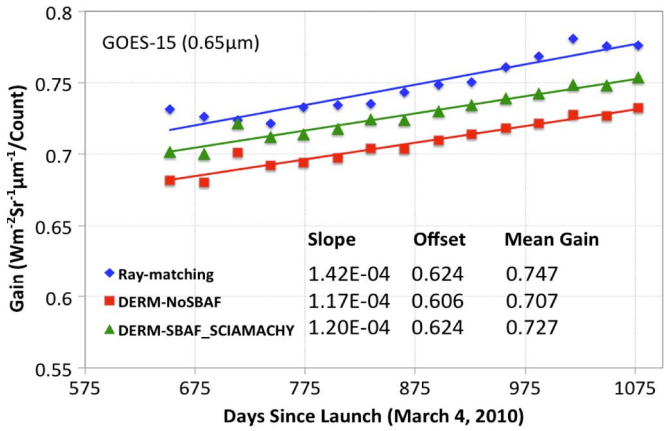

Fig. 14. Comparison of GOES-15 visible channel (0.65 μm) monthly radiometric gains derived from (blue diamonds) Aqua-MODIS/GOES-15 ray matching and (red squares) GOES-11 reference Sonoran Desert DERM with SBAF. The application of SCIAMACHY-based SBAF reduces the bias between the two approaches.

limit (3.06%) of the DERM approach for GOES-15. Therefore, it can be concluded that the SCIAMACHY footprints over the Sonoran Desert can be used to effectively reduce the radiometric difference between the reference and target GOES sensors caused by their spectral band differences. Investigations are ongoing to improve the uncertainty in the GOES sensor calibration using the DERM approach.

IV. Conclusion

PICSs have long served as benchmarks for assessing the postlaunch radiometric calibration of optical satellite sensors. Their use for relative trending or monitoring stability of the radiometric gain of a satellite sensor has been well accepted. A calibration approach using PICS as a reference for successive GEOs positioned at the same location with similar imaging schedules has been described. This approach allows for the construction of a reference DERM of PICS using the consistent-time daily observations from a well-calibrated GEO sensor. The reference GEO calibration was obtained from intercalibrating with Collection-6 Aqua-MODIS 0.65-μm channel data using coincident ray-matched radiances. Local noontime data were picked to maximize the SNR. A simple spatial threshold was applied to the standard deviation of the pixel-level TOA radiances over the PICS to determine if the site was clear for each day.

The use of the DERM assumes that the combined surface and clear-sky atmosphere column is invariant over multiple years for a given day of year, with a minimal year-to-year variability in the TOA radiance. This assumption was verified by constructing DERMs for Meteosat-9 and GOES-11 visible channels over the Libya-4 and Sonoran Desert PICSs, respectively. The average annual variability of the DERM radiance over Libya 4 and the Sonoran Desert is 0.74% and 1.20%, respectively. In order to account for any spectral band differences between a reference GEO and its predecessor, SBAFs were derived using the PICS-specific reflected solar spectra, obtained from SCIAMACHY hyperspectral observations. Because the SCIAMACHY 30-km-by-240-km footprint is much larger than the Libya-4 ROI, the potential impact of the spatial mismatch on the SBAF has been studied and found to be insignificant. The temporal stability of the PICS is the minimum requirement of this method, being that the calibration transfer is only as good as the quality of the PICS. PICSs were identified using Aqua-MODIS nadir reflectances over all GEO domains. The clear-sky DERM has the potential to calibrate historical, current, and future GEO sensors to the same calibration reference.

To validate the DERM approach, four self-consistency checks were performed. For the first case, the Meteosat-9 (reference) and Meteosat-8 (target) geostationary sensors had nearly identical SRFs and imaging schedules. The Libya-4 DERM calibration was applied to Meteosat-8 and was compared to the Aqua-MODIS ray-matched intercalibration gain during 2004 and 2007. The resulting calibration transfer is within 0.2%, which is well within the uncertainty of either methods. For both the reference and target period, the linear regression of the DERM monthly gain standard error is less than 0.6%, which suggests that the Libya-4 PICS is stable, as well as having a high surface reflectance and high spatial uniformity.

The second check also uses the Libya-4 PICS, but in this case, the MODIS-like SRF of Meteosat-9 is rather different than the nearly broad-band Meteosat-7 SRF, which contains many water vapor absorption bands. The Libya-4 DERM calibration and SCIAMACHY-based SBAF were applied to Meteosat-7 and compared with the ray-matched intercalibration based on Aqua MODIS. The intercalibration consistency is less than 1.9% between the DERM and ray-matching methods and is within their uncertainty. The linear regression of the Meteosat-7 DERM monthly gain standard error is 0.91%, which is almost twice as high as that for Meteosat-8, thus implying that almost half of the variability is from the atmospheric column.

The third case evaluates the Sonoran Desert site, which, when compared to Libya 4, has a lower surface reflectance, a smaller ROI, greater spatial variance, and slightly greater interannual daily variability. The GOES-11 (reference) DERM was first applied to GOES-10 (target) and compared with the corresponding Aqua-MODIS ray-matched intercalibration. The calibration consistency is 0.95%, again within the uncertainty of either intercalibration methods. The Sonoran Desert PICS navigation uncertainty was 0.4% given a 2-km shift, which is greater than the 0.1% for Libya 4 given a 3-km shift. The standard error of the linear regression of the monthly GOES-10 DERM gains was 0.83%. Most of this uncertainty is attributed to the temporal stability of the combined desert and atmosphere system being that the SRFs are somewhat similar.

The fourth case uses GOES-15 as a target GEO and GOES-11 DERM as a reference and also evaluates the effectiveness of the SCIAMACHY-based SBAF over the Sonoran Desert. The SCIAMACHY footprints over the Sonoran Desert are partially contaminated with surrounding vegetation and other surface types. The impact of these foreign surface types in the measured reflectance spectra is believed to be minimal. The GOES-15-to-GOES-11 SBAF had the highest uncertainty of all four cases, which is most likely a result of the lack of a seasonal SBAF due to inadequate SCIAMACHY sampling over the Sonoran Desert PICS. The application of SBAF reduces the systematic bias between the ray-matching and DERM calibration methods from 5.4% down to 2.7%, signifying

considerable improvement in the DERM approach. The remaining difference between the two approaches is, nonetheless, within the DERM calibration uncertainty. It is anticipated that the DERM calibration method can be applied to most historic and future GEO sensors to produce a consistent GEO observation record.

ACKNOWLEDGMENT

The National Aeronautics and Space Administration (NASA) Satellite Intercalibration Consistency Program and NASA Clouds and the Earth's Radiant Energy System mission to calibrate geostationary sensors supported this study. The authors would like to thank J. Xiong and the MODIS team for the assistance with the MODIS data. The MODIS data were obtained from the NASA Langley Distributed Active Archive Center. The geostationary Earth observing satellite data were obtained from the University of Wisconsin Space Science and Engineering Center, Madison, WI, USA. This study could not have been completed without the SCanning Imaging Absorption spectroMeter for Atmospheric CartograpHY (SCIAMACHY) data provided by the European Space Agency Environmental Satellite program. The authors would also like to thank J. Burrows, S. Noel, and K. Bramstedt at Bremen University, R. Snel at the Netherlands Institute for Space Research, and C. Lukashin at the NASA Langley Research Center for their assistance with the SCIAMACHY data.

REFERENCES

[1] W. B. Rossow and R. A. Schiffer, "Advances in understanding clouds from ISCCP," *Bull. Amer. Meteorol. Soc.*, vol. 80, no. 11, pp. 2261–2287, Nov. 1999.

[2] D. R. Doelling, N. G. Loeb, D. F. Keyes, M. L. Nordeen, D. Morstad, C. Nguyen, B. A. Wielicki, D. F. Young, and M. Sun, "Geostationary enhanced temporal interpolation for CERES flux products," *J. Atmos. Ocean. Technol.*, vol. 30, no. 6, pp. 1072–1090, Jun. 2013.

[3] P. Koepke, "Vicarious satellite calibration in the solar spectral range by means of calculated radiances and its application to Meteosat," *Appl. Opt.*, vol. 21, no. 15, pp. 2845–2854, Aug. 1982.

[4] H. Cosnefroy, M. Leroy, and X. Briottet, "Selection and characterization of Saharan and Arabian desert sites for the calibration of optical satellite sensors," *Remote Sens. Environ.*, vol. 58, no. 1, pp. 101–114, Oct. 1996.

[5] P. M. Teillet, J. A. Barsi, G. Chander, and K. J. Thome, "Prime candidate Earth targets for the post-launch radiometric calibration of satellite sensors," *Proc. SPIE*, vol. 6677, p. 66770S, 2007.

[6] R. J. Frouin and J. J. Simpson, "Radiometric calibration of GOES-7 VISSR solar channels during GOES pathfinder benchmark period," *Remote Sens. Environ.*, vol. 52, no. 2, pp. 95–115, May 1995.

[7] C. Moulin, C. E. Lambert, J. Poitou, and F. Dulac, "Long term (1983–1994) calibration of the Meteosat solar (VIS) channel using desert and ocean targets," *Int. J. Remote Sens.*, vol. 17, no. 6, pp. 1183–1200, 1996.

[8] Y. M. Govaerts and M. Clerici, "Evaluation of radiative transfer simulation over bright desert calibration sites," *IEEE Trans. Geosci. Remote Sens.*, vol. 42, no. 1, pp. 176–187, Jan. 2004.

[9] H. Chun, B. J. Sohn, D. Kim, and M. Ahn, "Solar channel calibration using desert targets in Australia," *J. Meteorol. Soc. Jpn.*, vol. 90, no. 2, pp. 191–205, 2012.

[10] P. Minnis, L. Nguyen, D. R. Doelling, D. F. Young, and W. F. Miller, "Rapid calibration of operational and research meteorological satellite images, Part I: Evaluation of research satellite visible channels as references," *J. Atmos. Ocean. Technol.*, vol. 19, no. 9, pp. 1233–1249, Sep. 2002.

[11] D. L. Morstad, D. R. Doelling, R. Bhatt, and B. Scarino, "The CERES calibration strategy of the geostationary visible channels for CERES cloud and flux products," in *Proc. SPIE*, *Earth Observing Syst. XVI*, 2011, p. 815 316.

[12] S. Kizu and H. Kawamura, "Degradation of the VISSR visible sensor on GMS-3 during June 1987–December 1988," *J. Atmos. Ocean. Technol.*, vol. 10, no. 4, pp. 509–517, Aug. 1993.

[13] J. Grau and R. Torres, "Drift in the Meteosat-7 VIS channel calibration," *Int. J. Remote Sens.*, vol. 23, no. 24, pp. 5277–5282, Jan. 2002.

[14] P. Le Borgne, G. Legendre, and A. Marsouin, "Meteosat and GOES-East imager visible channel calibration," *J. Atmos. Ocean. Technol.*, vol. 21, no. 11, pp. 1701–1709, Nov. 2004.

[15] G. Chander, X. Xiong, T. Choi, and A. Angal, "Monitoring on-orbit calibration stability of the Terra MODIS and Landsat 7 ETM+ sensors using pseudo-invariant test sites," *Remote Sens. Environ.*, vol. 114, no. 4, pp. 925–939, Apr. 2010.

[16] D. L. Helder, B. Basnet, and D. L. Morstad, "Optimized identification of worldwide radiometric pseudo-invariant calibration sites," *Can. J. Remote Sens.*, vol. 36, no. 5, pp. 527–539, Oct. 2010.

[17] A. Angal, X. Xiong, T. Choi, G. Chander, and A. Wu, "Using the Sonoran and Libyan Desert test sites to monitor the temporal stability of reflective solar bands for Landsat 7 enhanced thematic mapper plus and Terra moderate resolution imaging spectroradiometer sensors," *J. Appl. Remote Sens.*, vol. 4, no. 1, p. 043524, Apr. 2010.

[18] S. F. Staylor and J. T. Suttles, "Reflection and emission models for deserts derived from Nimbus-7 ERB scanner measurements," *J. Climate Appl. Meteorol.*, vol. 25, no. 2, pp. 196–202, Feb. 1986.

[19] D. L. Smith, C. T. Mutlow, and C. R. Nagaraja Rao, "Calibration monitoring of the visible and near-infrared channels of the along-track scanning radiometer-2 by use of stable terrestrial sites," *Appl. Opt.*, vol. 41, no. 3, pp. 515–523, Jan. 2002.

[20] D. L. Helder, S. Karki, R. Bhatt, E. Micijevic, and D. Aaron, "Radiometric calibration of the Landsat MSS sensor series," *IEEE Trans. Geosci. Remote Sens.*, vol. 50, no. 6, pp. 2380–2399, Jun. 2012.

[21] *CEOS WGCV Calibration and Validation Portal*. [Online]. Available: http://calvalportal.ceos.org

[22] A. Angal, G. Chander, X. Xiong, T. Choi, and A. Wu, "Characterization of the Sonoran desert as a radiometric calibration target for Earth observing sensors," *J. Appl. Remote Sens.*, vol. 5, no. 1, p. 059502, Jul. 2011.

[23] A. Wu, X. Xiong, D. R. Doelling, D. L. Morstad, A. Angal, and R. Bhatt, "Characterization of Terra and Aqua MODIS VIS, NIR, and SWIR spectral band calibration stability," *IEEE Trans. Geosci. Remote Sens.*, vol. 51, no. 7, pp. 4330–4338, Jul. 2013.

[24] C. R. N. Rao, N. Shang, and J. T. Sullivan, "Inter-calibration of meteorological satellite sensors in the visible and near-infrared," *Adv. Space Res.*, vol. 28, no. 1, pp. 3–10, 2001.

[25] Y. Zhang, B. Zhong, Q. Liu, H. Li, and L. Sun, "BRDF of Badain Jaran Desert retrieval using Landsat TM/ETM+ and ASTER GDEM data," in *Proc. IEEE IGARSS*, Jul. 24–29, 2011, pp. 1818–1821.

[26] A. Wu and Q. Zhong, "A method for determining the sensor degradation rates of NOAA AVHRR channels 1 and 2," *J. Climate Appl. Meteorol.*, vol. 33, no. 1, pp. 118–122, Jan. 1994.

[27] *GSICS Report in Comparison of Vicarious Calibration Methods and a Strategy to Use Various Land Sites for Inter-Comparison*, CGMS-38, NOAA-WP-26. [Online]. Available: ftp://ftp.eumetsat.int/pub/CPS/out/CGMS%2038%20report/CGMS-38%20CD/Working%20Papers%20CGMS-38/NOAA/CGMS-38%20NOAA-WP-26.pdf.

[28] P. Henry, D. Blumstein, D. Jouglet, and T. Colin, "Study of Asian and Australian desert sites for sensor cross-calibration in the VPIR range," in *Proc. Annu. GRWG+GDWG Meet.*, Daejeon, South Korea, Mar. 22–25, 2011.

[29] M. Schmidt, E. A. King, and T. R. McVicar, "A method for operational calibration of AVHRR reflective time series data," *Remote Sens. Environ.*, vol. 112, no. 3, pp. 1117–1129, Mar. 2008.

[30] J. L. Roujean, M. J. Leroy, and P. Y. Deschamps, "A bidirectional reflectance model of the Earth's surface for the correction of remote sensing data," *J. Geophys. Res.*, vol. 97, no. D18, pp. 20 455–20 468, Dec. 1992.

[31] D. R. Doelling, C. Lukashin, P. Minnis, B. Scarino, and D. Morstad, "Spectral reflectance corrections for satellite intercalibrations using SCIAMACHY data," *IEEE Geosci. Remote Sens. Lett.*, vol. 9, no. 1, pp. 119–123, Jan. 2012.

[32] *EUMETSAT MSG Calibration Webpage*. [Online]. Available: http://www.eumetsat.int/Home/Main/DataProducts/Calibration/MSGCalibration/index.htm?l=en

[33] X. Xiong, J. Sun, A. Wu, K. Chiang, J. Esposito, and W. Barnes, "Terra and Aqua MODIS calibration algorithms and uncertainty analysis," in *Proc. SPIE*, 2005, vol. 5978, p. 59 780V.

[34] *NOAA Satellite and Information Service Website*. [Online]. Available: http://www.oso.noaa.gov/goes/goescalibration/gvar-conversion.htm

Rajendra Bhatt received the B.S. degree in electronics engineering from Tribhuvan University, Kirtipur, Kathmandu, Nepal, in 2002 and the M.S. degree in electrical engineering from South Dakota State University (SDSU), Brookings, SD, USA, in 2009. At SDSU, he has studied the long-term radiometric stability of and calibrated the Landsat-1 through Landsat-5 Multispectral Scanner System sensors using pseudoinvariant calibration sites.

He is currently employed by Science Systems and Applications, Inc., Hampton, VA, USA, as a Contract Research Scientist to support the Clouds and Earth's Radiant Energy System project at the National Aeronautics and Space Administration Langley Research Center, where he is developing techniques of in-flight calibration of satellite visible and infrared observations to assess the sensor's performance on orbit and ensure the usability of climate data.

David R. Doelling received the B.S. degree in meteorology from the University of Utah, Salt Lake City, UT, USA, in 1985 and the M.S. degree in atmospheric science from the University of Washington, Seattle, WA, USA, in 1991.

He is currently a Senior Research Scientist at the National Aeronautics and Space Administration (NASA) Langley Research Center, Hampton, VA, USA, where he is the Time Interpolation and Spatial Averaging Sublead for the Clouds and Earth's Radiant Energy System (CERES) project and responsible for the diurnal averaging and spatial gridding of CERES footprint cloud and radiative flux parameters. He is also a member of the Geostationary Earth Radiation Budget Experiment and Megha-Tropique science teams, projects similar to CERES that measure broad-band fluxes. He has studied the orbital sampling errors for proposed satellites as a member of the Climate Absolute Radiance and Refractivity Observatory science definition team. He is the Global Space-based Inter-Calibration System NASA representative and the Lead for geostationary/MODIS ray-matching and deep convective cloud visible calibration methods. His research interests include geostationary imager calibration, diurnal averaging techniques of satellite observations, and satellite sampling studies.

Daniel Morstad received the B.S. and M.S. degrees in electrical engineering from South Dakota State University, Brookings, SD, USA, in 2007 and 2009, respectively. His graduate research focused on the development of a statistically based automation technique for selecting the most temporally invariant Earth targets based on the Landsat-5 Thematic Mapper data record.

He is currently a Research Scientist at Science Systems and Applications, Inc., Hampton, VA, USA, in support of the Clouds and Earth's Radiant Energy System (CERES) project at the National Aeronautics and Space Administration Langley Research Center, Hampton, VA, USA. He is primarily responsible for maintaining the real-time geostationary visible sensor calibration record and is currently developing a deep convective cloud absolute calibration technique that will be vital to the uniform radiometric calibration of both past and future Earth-observing sensors.

Benjamin R. Scarino received the M.S. degree in meteorology from the Pennsylvania State University, State College, PA, USA, in 2010.

Shortly thereafter, he was hired by Science Systems and Applications, Inc., Hampton, VA, USA, as a Staff Research Scientist. There, he supports the Clouds and the Earth's Radiant Energy System Project, working on cloud and radiation data-set development and on-orbit calibration.

Arun Gopalan received the B.S degree in mechanical engineering from Victoria Jubilee Technical Institute, University of Bombay, Mumbai, India, in 1991 and the M.S. degree in mechanical engineering from the State University of New York, Stony Brook, NY, USA, in 1993, where he completed all Ph.D. requirements excluding dissertation defense as of 1997. His dissertation focused on the research and development of an optimal retrieval algorithm for the simultaneous extraction of diurnal stratospheric nitrogen dioxide and aerosol extinction profiles using Earth-limb Infrared Emission measurements from the National Aeronautics and Space Administration (NASA)'s Upper Atmospheric Research Satellite Cryogenic Limb Array Etalon Spectrometer instrument.

He is currently a Senior Research Scientist with Science Systems and Applications, Inc., based at Hampton, VA, USA, in support of the NASA Langley Research Center's Cloud and Earth's Radiant Energy System and Climate Absolute Radiance and Refractivity Observatory projects. He has previously coauthored a number of journal papers and worked in the area of satellite remote sensing for over 15 years with earth science research groups at the NASA Goddard Space Flight Center, Greenbelt, MD, USA, and National Center for Atmospheric Research, Boulder, CO, USA. His research interests include studies of postlaunch calibration techniques to understand satellite sensor performance, science retrieval algorithm development, remotely sensed data processing methods, aerosol–cloud–climate feedback mechanisms, visualization of large-scale earth science data sets, and data mining.